Supplementary Material :

APPENDIX A:

The day (a continuous interval from sunrise ($t = 0$) to sunset ($t = 1$)) is split into smaller time intervals at the start of the day. These intervals are defined by the temporal position of ***known*** events.

- ***Known*** events are the transitions from resting to reproductive activity (and *vice versa*) for every individual, as well as the emergence of new adult individuals. The number of known events is thus at least 2*Number of individuals + Number of emerging individuals.

A second type of stochastic event can happen between two *known* events, which are ***unknown*** events.

- ***Unknown*** events are dependent on the state of the population at a certain moment in time, such as *mating* or *death* events. The individual involved in an event is randomly chosen, uniformly among individuals exhibiting the same status. The time at which those events happen is drawn in an exponential distribution, based on the current numbers of active males $\mathbf{N_a}^{\male}$, resting males $\mathbf{N_r}^{\male}$, available active females $\mathbf{N_a}^{\female}$, resting available females $\mathbf{N_r}^{\female}$, and unavailable females $\mathbf{N_m}^{\female}$. We continue drawing new mating or death events until the drawn time exceeds the time of the next known event. At that point, the known event is prioritized and takes place instead.

Unknown events occurrence times and rates are computed using the instantaneous mating rate λ_r and the instantaneous death rate λ_d, given by:

$$\lambda_r = \beta * N_a^{\female} * N_a^{\male} \quad (1)$$

$$\lambda_d = d * (N_a^{\male} + N_r^{\male} + N_a^{\female} + N_r^{\female} + N_m^{\female}) + \delta_e * (N_a^{\male} + N_a^{\female}) + \delta_c * N_a^{\male} * (N_a^{\male}-1) + \delta_l * \sum_{i=0}^{N_m^{\female}} E_i \quad (2)$$

The time at which those events happen is drawn in an exponential distribution of parameter $\frac{1}{\lambda r+\lambda d}$. If this occurring time is smaller than the occurring time of the next known event, then a mating or a death event happens. If this occurring time is higher than the occurring time of the

next event, nothing happens except the next known event. To determine which event between mating and death occurs, a value is drawn from a uniform distribution $U(0,1)$ and is compared to $\frac{\lambda r}{\lambda r+\lambda d}$. If the value drawn is smaller, then a mating event occurs. If not, we compare it with $\frac{\lambda r}{\lambda r+\lambda d}. + \frac{d^* N_r^{\male}}{\lambda r+\lambda d}$, which corresponds to the death of an inactive male. If the value is still greater, we compare with $\frac{\lambda r}{\lambda r+\lambda d}. + \frac{d^* N_r^{\male}}{\lambda r+\lambda d} + \frac{(d+\delta_e)^* N_a^{\female}}{\lambda r+\lambda d}$ (death of an available active female), and so on.

In the case of unavailable females, we consider the number of eggs E_i laid by each individual.

As such, there are $\mathbf{N_m}^{\female}$ events we need to check:

We compare the value drawn from the uniform distribution to with:

- $\frac{\lambda r}{\lambda r+\lambda d} + \ldots + \frac{d+\delta_l * E_1}{\lambda r+\lambda d}$ for the death of unavailable female number 1;
- $\frac{\lambda r}{\lambda r+\lambda d} + \ldots + \frac{2d+\delta_l *(E_1+E_2)}{\lambda r+\lambda d}$ for the death of unavailable females number 2;

and so on until the event of the death of unavailable female number $\mathbf{N_m}^{\female}$:

- $\frac{\lambda r}{\lambda r+\lambda d} + \ldots + \frac{(N_m^{\female} * d)+ \delta l * \sum_{i=1}^{N_m^{\female}} E_i}{\lambda r+\lambda d}$.

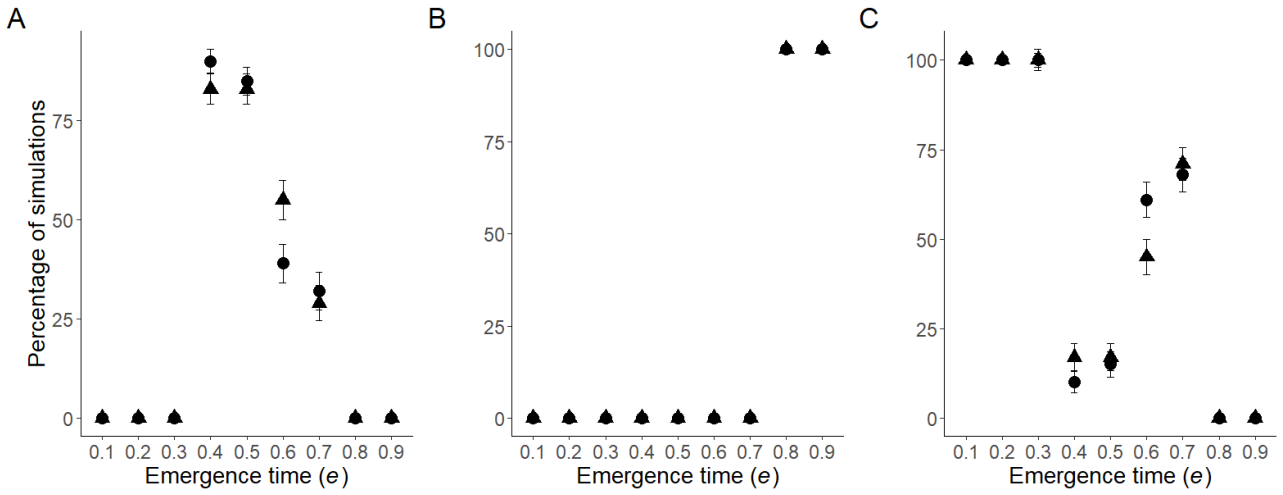

Figure S1:**Comparisons of simulation outcomes, after 500 vs. 2000 days.** Circles and triangles indicate simulation outcomes after 500 and 2000 days respectively. We run 100 simulations per condition, and distinguished them based on the distribution of the timing of reproductive activity h_a after 500 days. These distributions were either bimodal (A), delayed-dawn (B) or immediate (C). We observe similar patterns no matter the simulation length, we thus used 500-days outcomes for all analyses in this study.

Error bars represented by one standard deviation (SD). All simulations were run assuming the same parameter values: $\delta c = 0.1$, $\beta = 3$, $G = 1$, $e = 0.5$, $Ve = 0.05$, $p = 1$, $K=1000$.

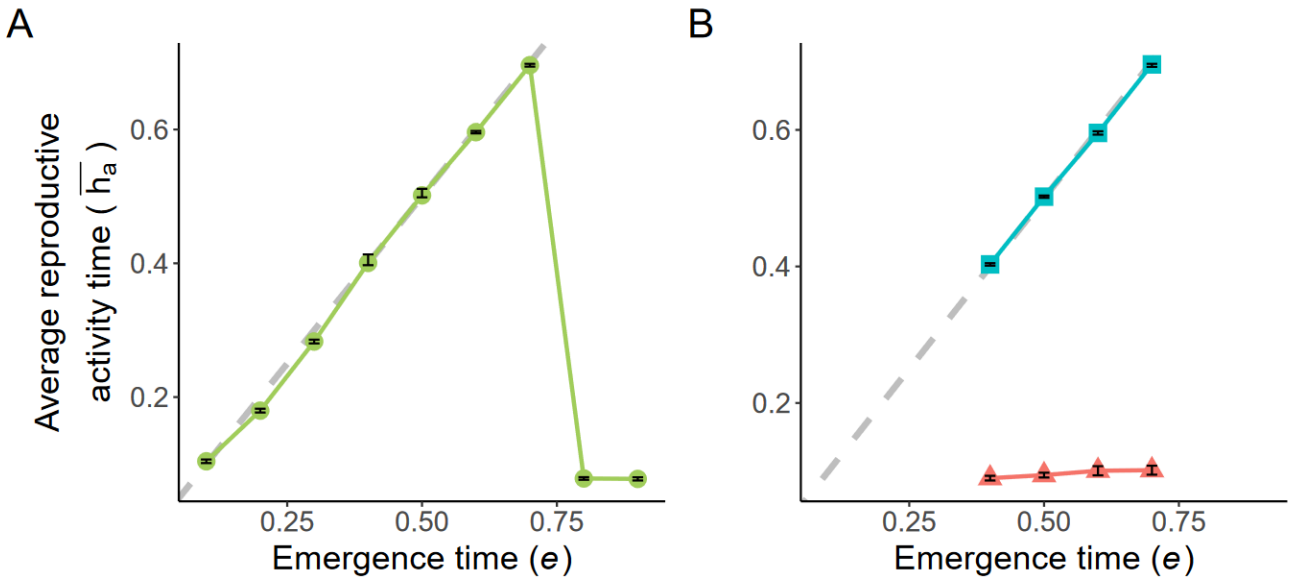

Figure S2: **Temporal niches in the sub-populations, depending on the timing of adult emergence**, estimated by the average reproductive activity timings, obtained in simulations assuming different values of the timing of emergence of adult e. We run 100 simulations per condition, and distinguished them based on the distribution of the timing of reproductive activity h_a after 500 days. These distributions were either unimodal (A) or a bimodal (B). In the bimodal case, dawn-shifted and immediate temporal niches can be observed, where the average ha within the sub-populations are shown in red triangles and blue squares respectively. Dashed lines then show the emergence time e in the corresponding simulations.
Error bars represented by one SD. All simulations were run assuming the same parameter values: δc = 0.1, β = 3, G = 1, Ve = 0.05, p = 1, K=1000.

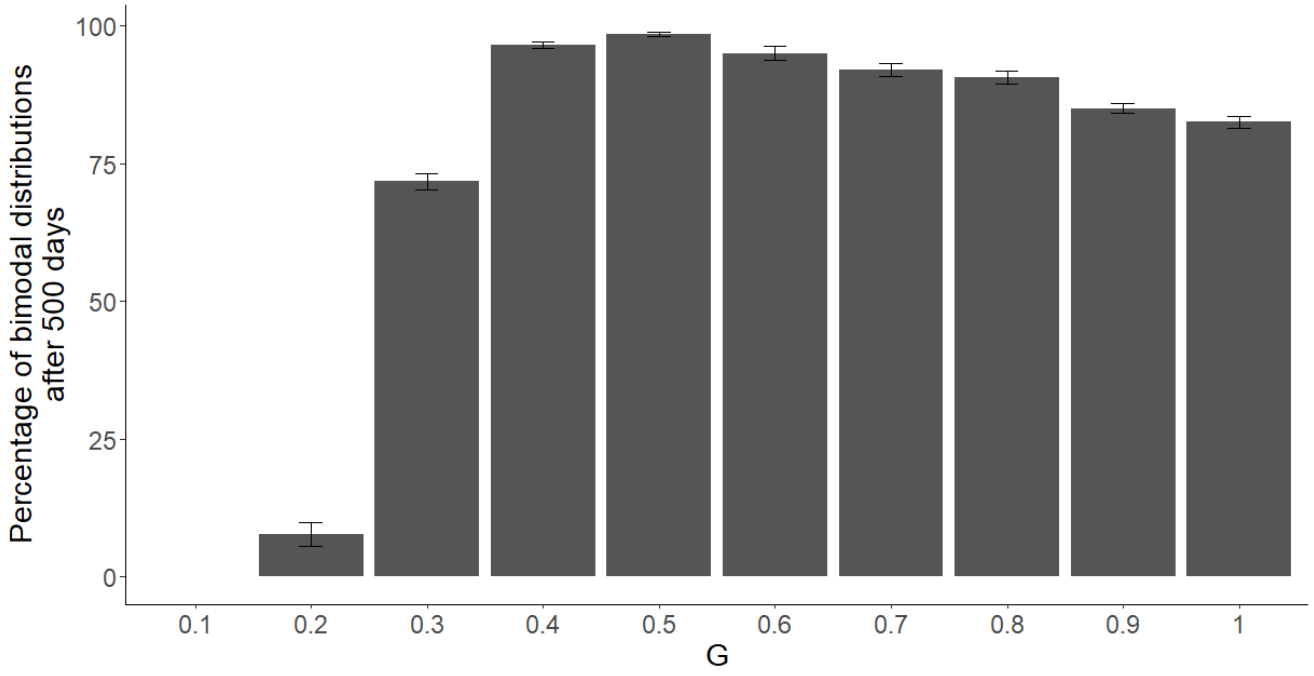

Figure S3: **Effect of the proportion of loci required to generate incompatibility (*G*) between individuals on the evolution of sub-populations with different temporal niches.** Percentage of simulations where a bimodal distribution in the timing of activities is observed at 500 days, depending on the proportion of loci G necessary to trigger incompatibility.
Error bars are one SD. All simulations were run assuming the same parameter values: $\delta c = 0.1$, $\beta = 3$, $e = 0.5$, $Ve = 0.05$, $p = 1$, $K=1000$.

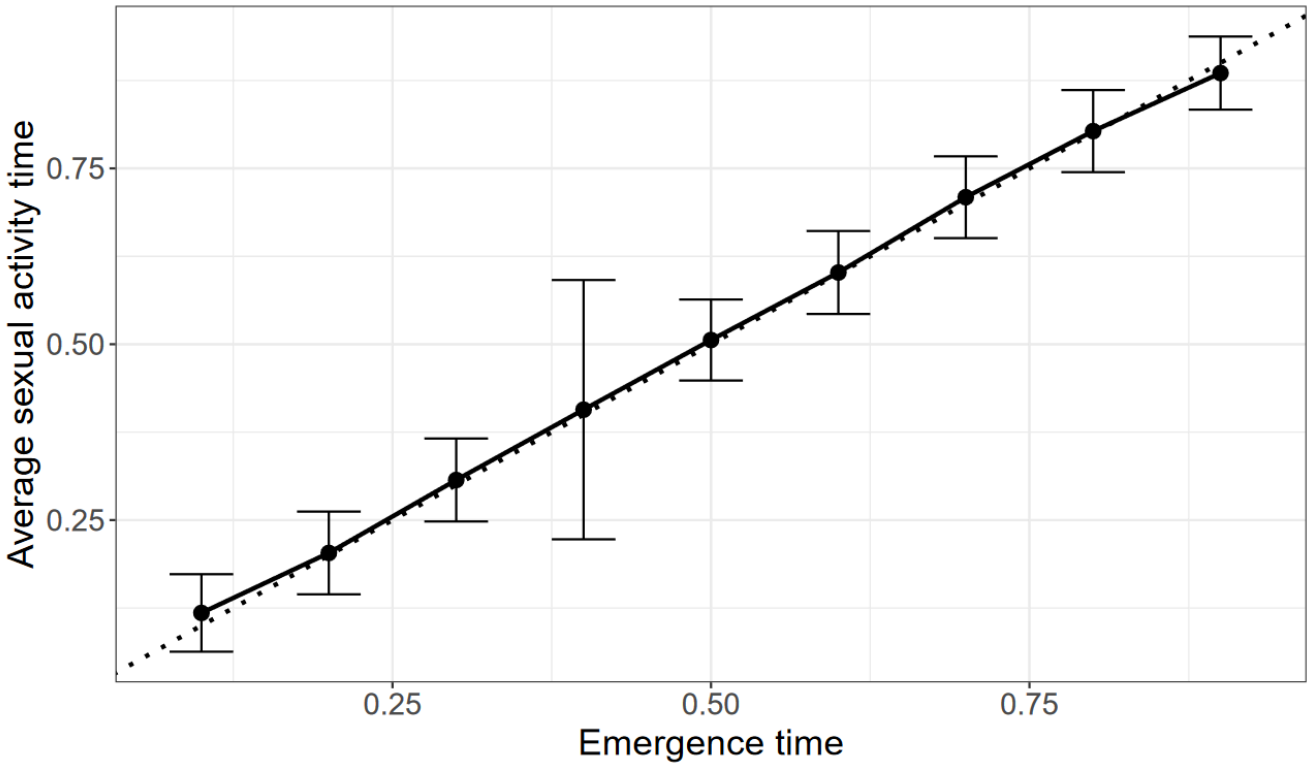

Figure S4: **Effect of the emergence time *e* on the average timing of reproductive activities in a *seasonal* model (*i.e.* assuming non-overlapping generations).** The dotted line shows the emergence timing. In the seasonal model, average activity times are centered around the time of emergence, and no bimodality is observed in the timing of reproductive activities, assuming low level of male-male competition.
Error bars are a 95% confidence interval. All simulations were run assuming the same parameter values: $\delta c = 0.1$, $\beta = 3$, $G = 0.4$, $Ve = 0.05$, $p = 1$, $K=1000$.

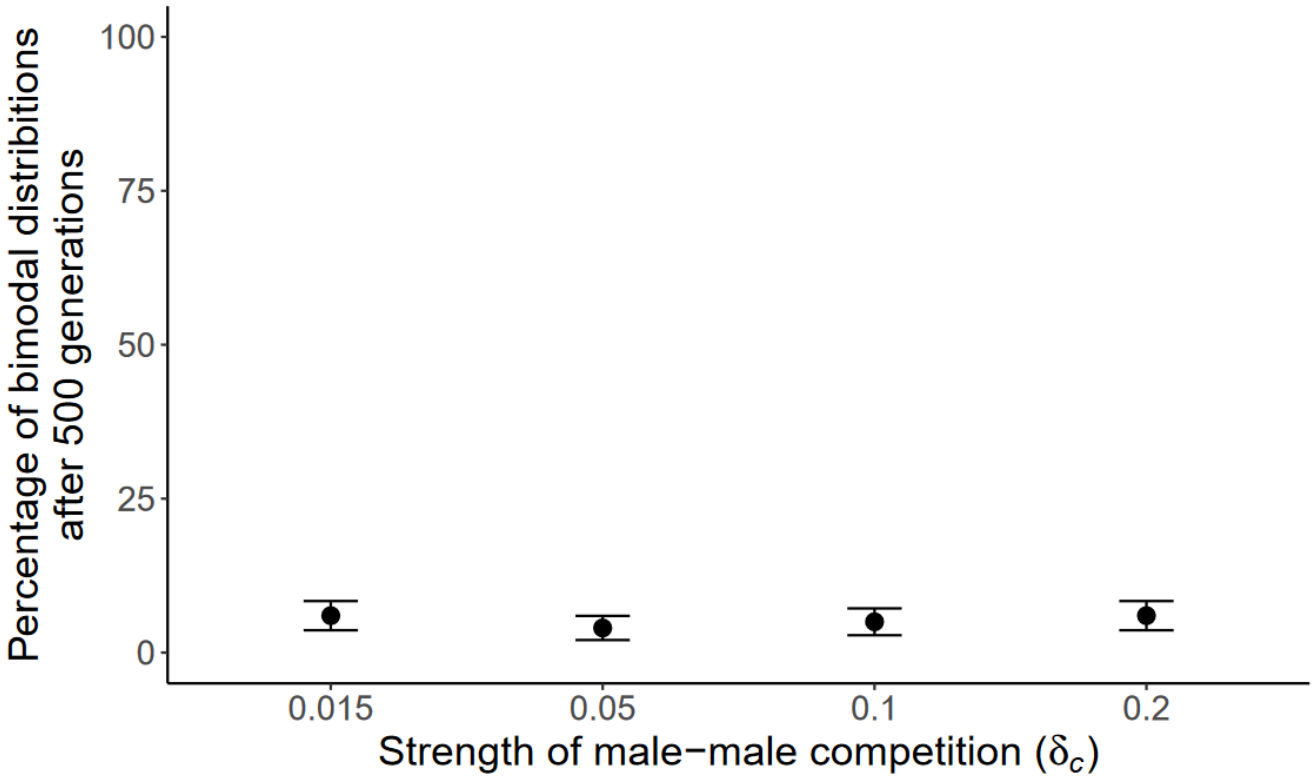

Figure S5: **Effect of low levels of male-male competition on the emergence of bimodal distribution in the activity time, in a *seasonal* model.** We can observe that male-male competition values generating bimodal distribution of reproductive activities on the daily model (see Figure 4A) barely produces any bimodal distribution in the activity timings in the seasonal model. Evolution of differentiated temporal niches indeed only happened in circa 5% of the simulations.
Error bars are one SD. All simulations were run assuming the same parameter values: $\beta = 3$, $G = 0.4$, $e = 0.5$, $Ve = 0.05$, $p = 1$, $K=1000$.

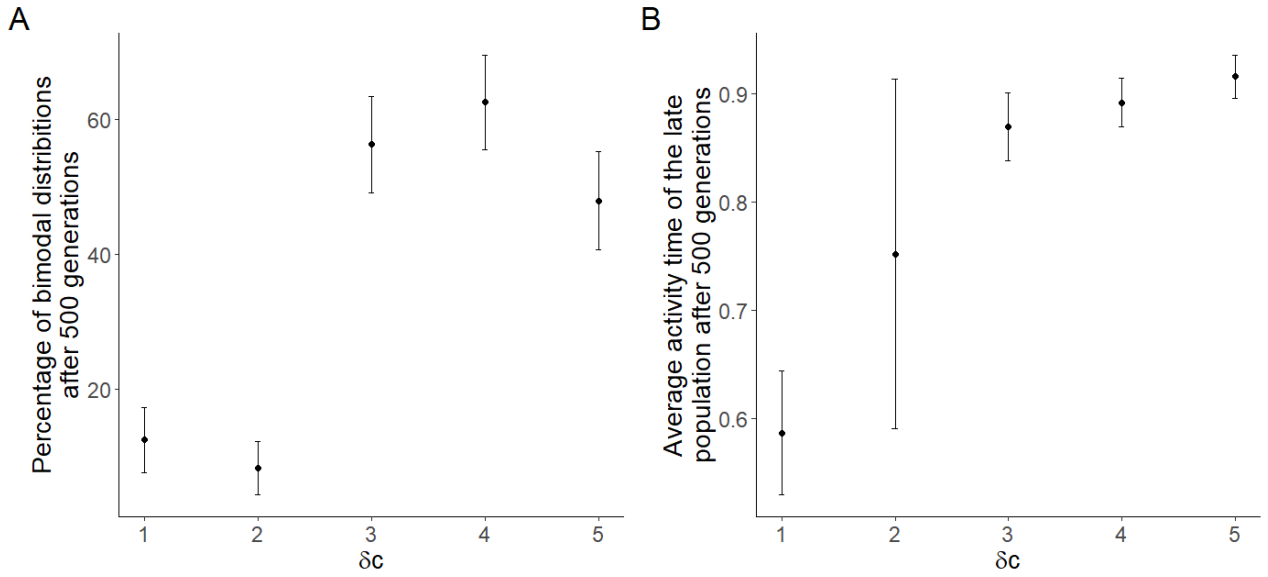

Figure S6: **Effect of male-male competition on the evolution of differentiated sub-populations in a *seasonal* model**. We run 100 simulations per condition, and distinguished them based on the distribution of the timing of reproductive activity h_a after 500 days. (A) Percentage of differentiated populations observed depending on the cost of male-male competition δc. High male-male competition can still produce frequent bimodality in the activity timings in a seasonal model, but only for extreme values of δc. (B) Temporal position of the sub-population with later reproductive activity in the seasonal model depending on the cost of male-male competition δc. We can observe that higher cost for male-male competition is correlated with later and later timings of reproductive activity for those sub-populations.

Error bars are one SD. All simulations were run assuming the same parameter values: $\beta = 3$, $G = 0.4$, $e = 0.5$, $Ve = 0.05$, $p = 1$, $K=1000$.

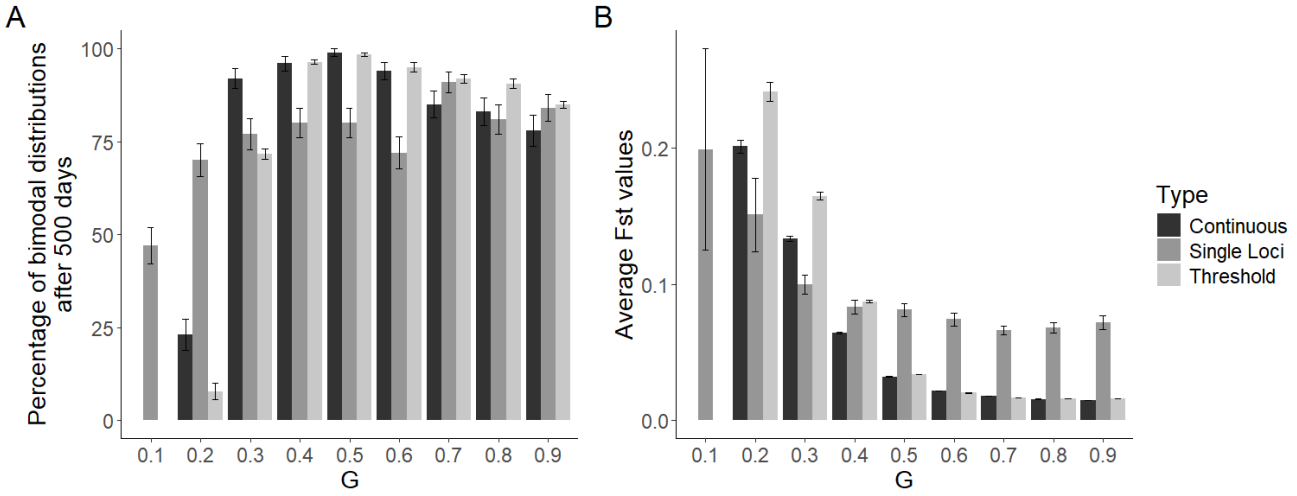

Figure S7: **Effect of the proportion of loci required to generate incompatibility on population differentiation (G) depending on the simulation type.** 100 simulations were run for each type of modelling variation. We characterised either (A) the percentage of simulation ending in a bimodal distribution of the reproductive activity timing and (B) the average Fst values between the two sub-populations. Three types of simulations are presented in the graphs above :

1. Threshold for a non-continuous effect of incompatibility alleles, where over a certain difference in genetic values of size G, no offspring are deemed viable. This is the current modelling approach.
2. *Continuous* for a continuous effect of incompatibility alleles, were the mean number of offspring is determined by a logistic function (with offspring number = 1 - $\frac{1}{1+e^{(-20*(difference\ in\ genetic\ values-G)}}$).
3. Single loci for a non-continuous effect of incompatibility alleles, with a single continuous genetic value representing the neutral genetic diversity, instead of a list of loci.

We observe qualitatively similar results for all modelling approaches, with slight differences in Fst values: the threshold model leads to higher Fst compared to the continuous model, while the single loci model has overall higher Fst values for higher G values.
Error bars are one SD. All simulations were run assuming the same parameter values: $\delta c = 0.1$, $\beta = 3$, $e = 0.5$, $Ve = 0.05$, $p = 1$, $K=1000$.

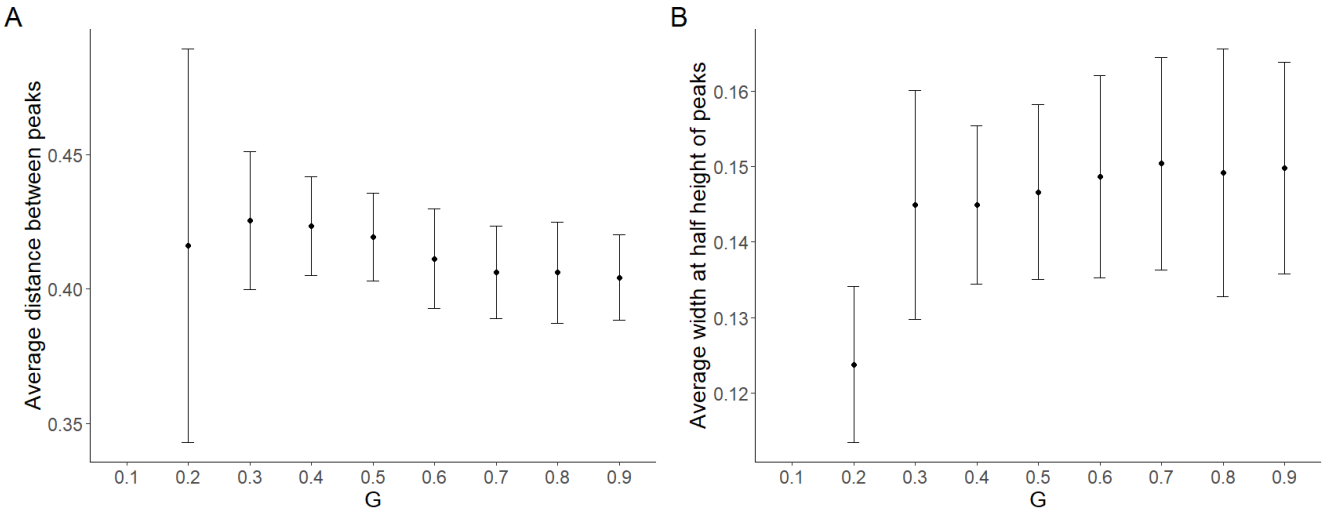

Figure S8: **Peaks characterization via distance between peaks and width of peaks, depending on the proportion of loci necessary to generate incompatibilities.** We run 100 simulations for each parameter, assessing the (A) average distance between peaks at the end of simulations, when two peaks were detected. We also measured (B) the average width of the peaks at half height, using a gaussian fit for each peak. This characterization ensured that our peaks did not overlap, and were far enough apart to be considered two differentiated sub-populations. For G=0.2, high variability in peak distance and smaller peak width might be caused by a smaller population size due to a stricter threshold on reproduction.
Error bars are one SD. All simulations were run assuming the same parameter values: $\delta c = 0.1$, $\beta = 3$, $e = 0.5$, $Ve = 0.05$, $p = 1$, $K=1000$.

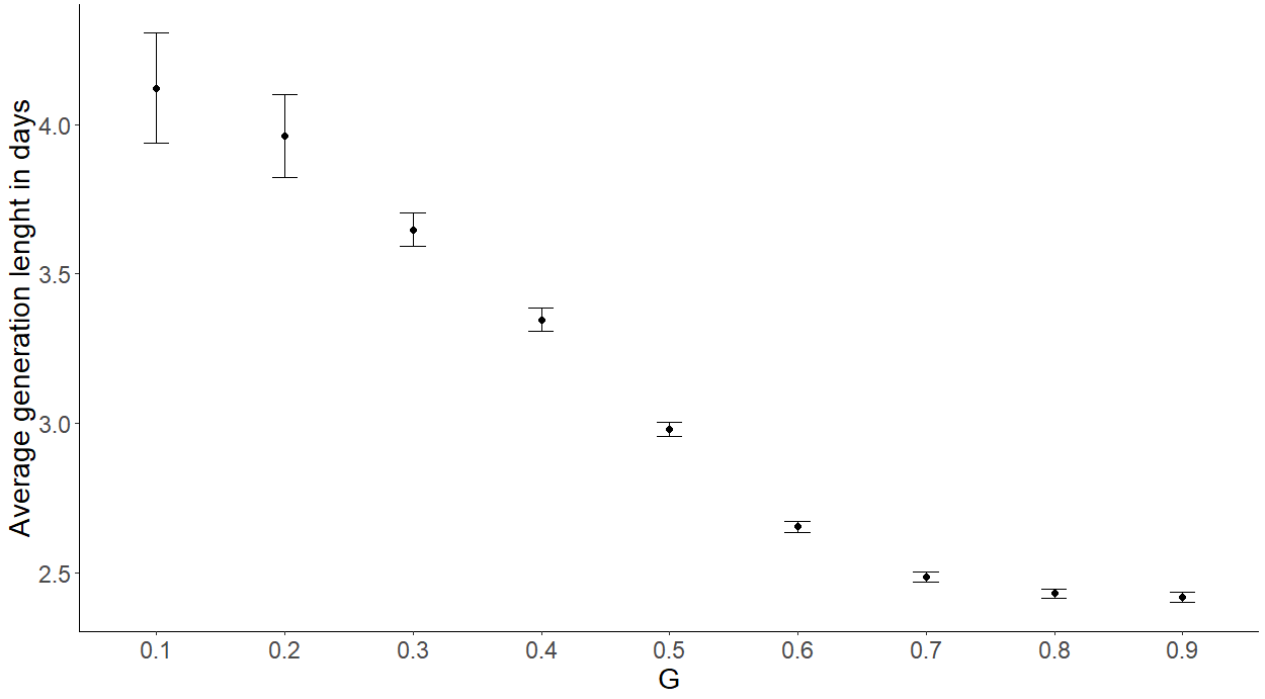

Figure S9: **Average generation time within simulation, depending on the proportion of loci necessary to generate incompatibilities.** We run 100 simulations per parameter, measuring the average length of a generation for each. Generation time is lowered as G rises, from 4 days to only 2.5. Error bars are one SD. All simulations were run assuming the same parameter values: $\delta c = 0.1$, $\beta = 3$, $e = 0.5$, $Ve = 0.05$, $p = 1$, $K=1000$.

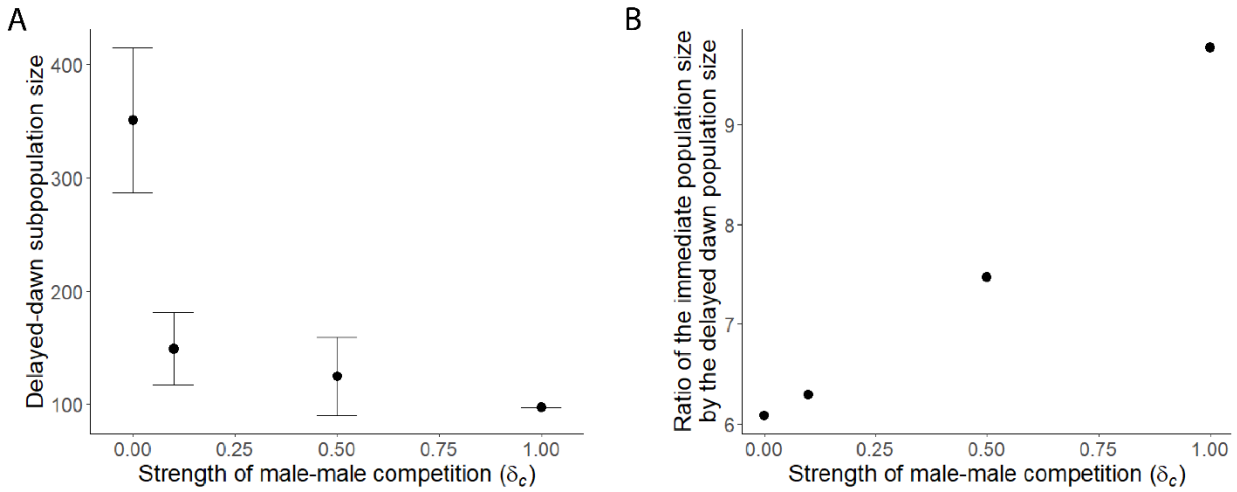

Figure S10: **Effect of male-male competition on the population size of delayed-dawn subpopulations.** We run 100 simulations per parameter. We characterized delayed-dawn sub-populations either by (A) their population size or (B) the ratio between the size of the delayed-subpopulation and the immediate sub-population. We can observe that higher male-male competition values correspond to smaller sized delayed-dawn, as well as a higher differential in size between immediate and delayed-dawn subpopulations.
Error bars are one SD. All simulations were run assuming the same parameter values: $\beta = 3$, $G = 1$, $e = 0.5$, $Ve = 0.05$, $p = 1$, $K=1000$.

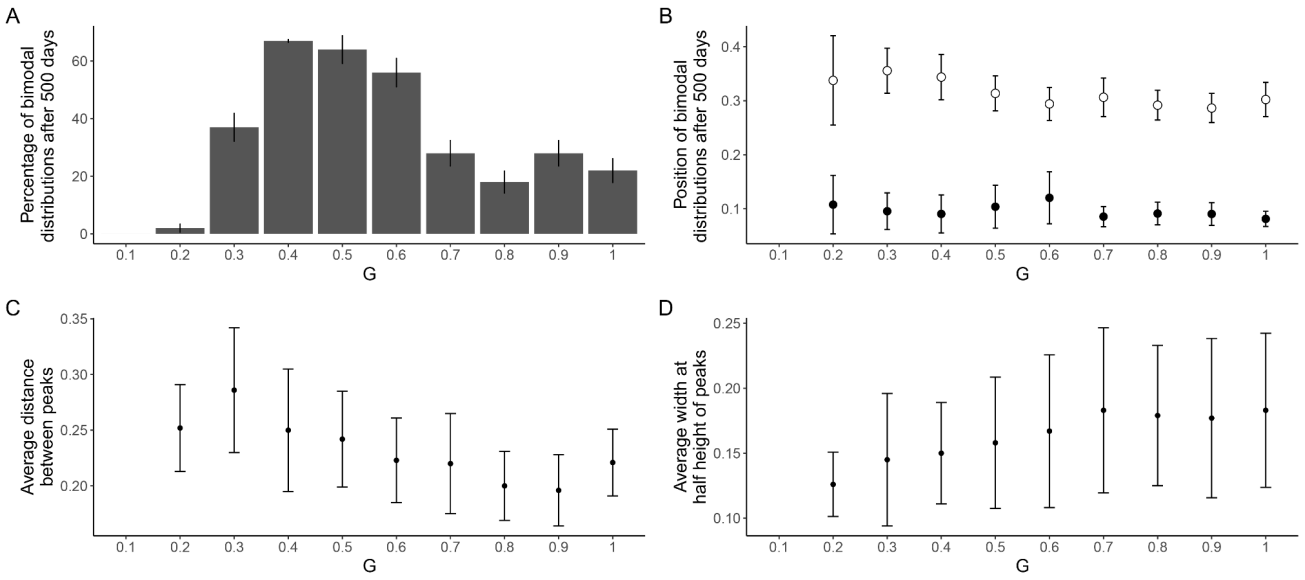

Figure S11: **Effect of the coevolution of sexual activity timings and emergence timing on the evolution of differentiated sub-populations in a *daily* model,** depending on the proportion of loci necessary to generate incompatibilities. Characterisation of the results of 100 simulations per parameter with coevolution of h_a and e are presented above with (A) the percentage of bimodal distributions after 500 days. (B) The position of peaks in reproductive activity timing, in simulations ending with a bimodal distribution of the h_a trait. (C) The average distance between the two peaks in reproductive activity timing, as well as (D) the average width at half height of those peaks. We observed differentiation when coevolution of h_a and e was allowed, albeit at a lower frequency than when e was fixed. Both sub-populations seem to display early activity, with little to no overlap in reproductive activity timing.
Error bars are one SD. All simulations were run assuming the same parameter values: $\delta_c = 0\ .1$, $\beta = 3$, $e = 0.5$, $V_e = 0.05$, $p = 1$, $K=1000$.

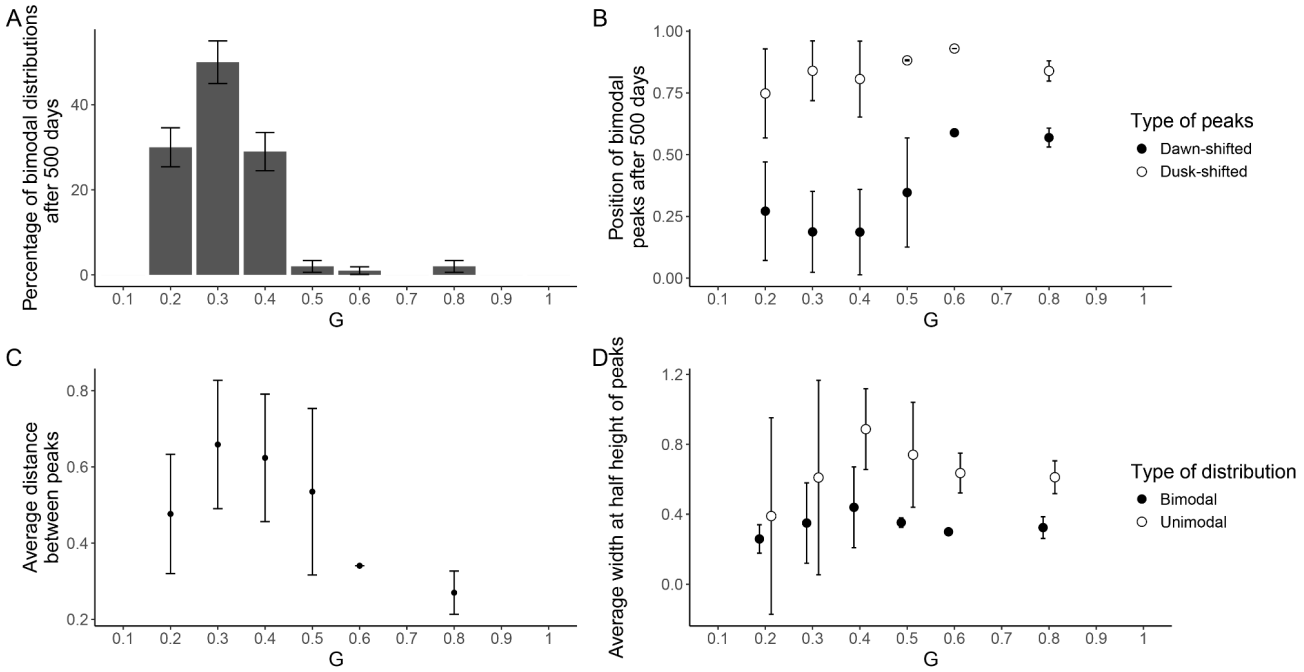

Figure S12: **Effect of differential evolution of the reproductive activity timing of males and females in a daily model.** Characterisation of the results of 100 simulations per parameter with sex-specific expression of the reproductive activity timing are presented above with (A) the percentage of bimodal distributions after 500 days. (B) The position of peaks in reproductive activity timing, in simulations ending with a bimodal distribution of the ha trait. (C) The average distance between the two peaks in reproductive activity timing, as well as (D) the average width at half height of those peaks, depending on the type of distribution. We can observe that only a narrow set of values of G allow for population differentiation, and that sub-populations were very spread out in activity timings by looking at the trait distribution. Notably, unimodal distributions tended to be more spread out than bimodal ones.

Error bars are one SD. All simulations were run assuming the same parameter values: $\delta_c = 0\ .1$, $\beta = 3$, $e = 0.5$, $V_e = 0.05$, $p = 1$, $K=1000$.

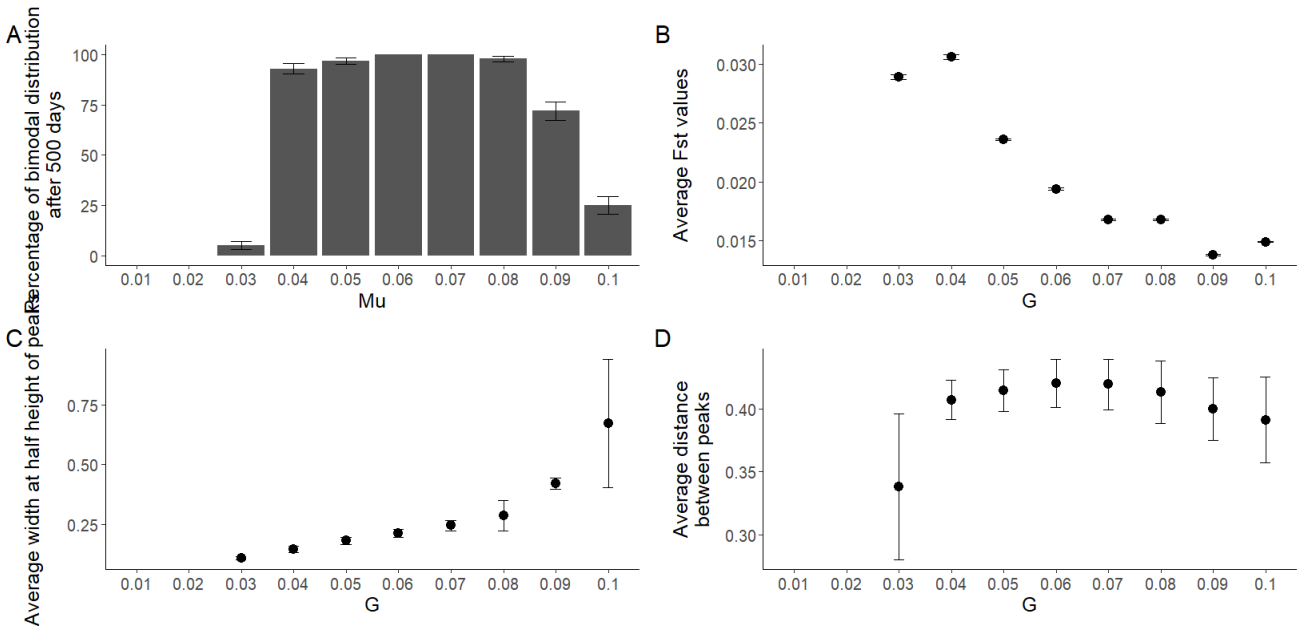

Figure S13: **Effect of the standard deviation μ of sexual activity timings on the evolution of differentiated sub-populations in a *daily* model,** depending on the proportion of loci necessary to generate incompatibilities. Characterisation of the results of 100 simulations per parameter is presented above with (A) the percentage of bimodal distributions after 500 days. (B) The average Fst between sub-populations after 500 days. (C) The average width at half height of the peaks in the distribution of the reproductive activity timing, as well as (D) the average distance between the two peaks in reproductive activity timing. We can observe that low values of μ tend to not allow for differentiation within the population to occur, while high values disrupt the population structure, making inheritance of the activity time too random. The spread in activity timing becomes very large, and F_{st} values drop significantly. Medium values on the other hand, allow for population differentiation based on activity time.
Error bars are one SD. All simulations were run assuming the same parameter values: $\delta_c = 0\ .1$, $\beta = 3$, $e = 0.5$, $V_e = 0.05$, $p = 1$, $K=1000$.

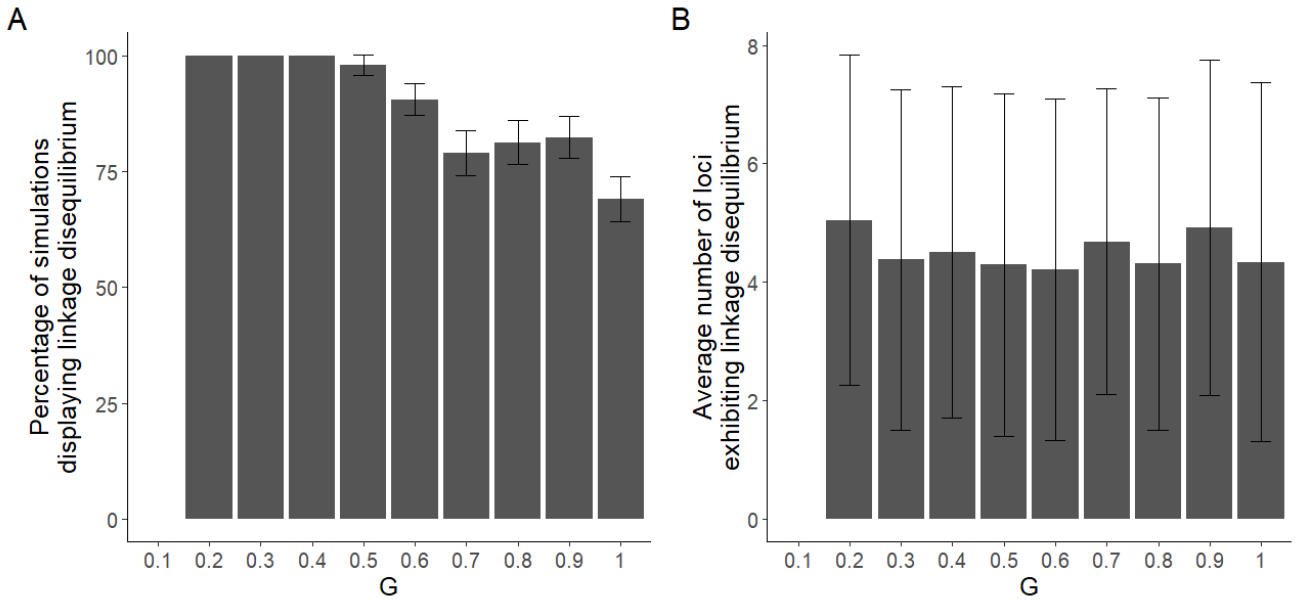

Figure S14: **Characterisation of linkage disequilibrium between activity time and the neutral genetic components, depending on the proportion of loci necessary to generate incompatibilities**. Using point-biserial correlation, we assessed the presence of linkage disequilibrium at each locus by testing whether the mean average reproductive activity differed significantly between individuals with a value of 1 and those with a value of 0 at this locus. We quantified (A) the percentage of simulations ending with differentiated sub-populations and displaying at least one locus with linkage disequilibrium, (B) the average number of loci exhibiting linkage disequilibrium when it arose. We can observe that for lower values of G, sub-populations exhibit linkage disequilibrium more frequently, but without a difference in the number of loci involved in this linkage disequilibrium. Stricter genetic incompatibilities are thus promoting more frequent linkage disequilibrium, but not a stronger one.
Error bars are one SD. All simulations were run assuming the same parameter values: $\delta_c = 0$ .1, $\beta = 3$, $e = 0.5$, $V_e = 0.05$, $p = 1$, $K=1000$.